

Chapter 3

Lithological control on the deformation mechanism and the mode of fault slip on the Longitudinal Valley Fault, Taiwan

Marion Y. Thomas, Jean-Pierre Gratier, Jean-Philippe Avouac, and Jian-Cheng Lee

Abstract

The Longitudinal Valley Fault (LVF) in Taiwan is creeping at shallow depth along its southern half, where it is bounded by the Lichi Mélange. By contrast, the northern segment of the LVF is locked where it is bounded by forearc sedimentary and volcanoclastic formations. Structural and petrographic investigations show that the Lichi Mélange most probably formed as a result of internal deformation of the forearc when the continental shelf of South China collided with the Luzon arc as a result of the subduction of the South China Sea beneath the Philippine Sea Plate. The forearc formations constitute the protolith of the Lichi Mélange. It seems improbable that the mechanical properties of the minerals of the matrix (illite, chlorite, kaolinite) in themselves explain the aseismic behavior of the LVF. Microstructural investigations show that deformation within the fault zone must have resulted from a combination of frictional sliding at grain boundaries, cataclasis (responsible for grain size comminution) and pressure solution creep (responsible for the development of the scaly foliation and favored by the mixing of soluble and insoluble minerals). The microstructure of the gouge formed in the Lichi Mélange favors effective pressure solution creep, which inhibits strain-weakening brittle mechanisms and is probably responsible for the dominantly aseismic mode of fault slip. Since the Lichi Mélange is analogous to any unlithified subduction mélanges, this study sheds light on the mechanisms which favor aseismic creep on subduction megathrust.

3.1 Introduction

Geodetic and seismological observations show that fault slip can be either seismic or aseismic. The observation that locked fault patches tend to coincide with seismic ruptures, combined with numerical studies, suggests that the partitioning between aseismic and seismic slip is an influential and perhaps determining factor governing the spatial extent, size and timing of earthquake ruptures (e.g., *Barbot et al.*, 2012; *Hsu et al.*, 2009a; *Kaneko et al.*, 2010; *Noda and Lapusta*, 2010; *Perfettini et al.*, 2010; *Harris and Segall*, 1987; *Hashimoto et al.*, 2009; *Loveless and Meade*, 2011; *Chlieh et al.*, 2008; *Moreno et al.*, 2010). However, the factors that determine the mode of fault slip, and hence the seismogenic potential of faults, are still poorly understood. Ascertaining those factors by defining the spatial and temporal variability of frictional properties, and understanding the deformation mechanisms and their relative importance are therefore major goals in seismotectonics.

We propose to address this problematic by investigating the deformation mechanisms that control aseismic slip on the Longitudinal Valley Fault (LVF) in Taiwan. This fault runs parallel to the East coast of Taiwan and defines the plate boundary between the Chinese continental margin, considered to be part of the Eurasian plate, and the oceanic Philippine Sea Plate (*Lee et al.*, 2001; *Chang et al.*, 2009) (Figure 3.1). This fault is known to creep near the surface (*Angelier et al.*, 1997; *Lee et al.*, 1998, 2000, 2001, 2005; *Chang et al.*, 2009; *Champenois et al.*, 2012; *Thomas et al.*, to be submitted) but has also produced large earthquakes, with five $M_w > 6.8$ events in 1951 and 2003 (*Shyu et al.*, 2007; *Wu et al.*, 2006a; *Hsu et al.*, 2009a; *Mozziconacci et al.*, 2009; *Thomas et al.*, to be submitted). Modeling of the spatio-temporal evolution of seismic and aseismic slip on the LVF, derived from the inversion of geodetic, remote-sensing and accelerometric data, has demonstrated that as much as 80-90% of the 4.5 cm/yr slip rate on the LVF, in the 0-26 km seismogenic depth range (as defined by local seismicity), is actually the result of aseismic creep (*Thomas et al.*, to be submitted). The spatial pattern of aseismic creep on the LVF is very heterogeneous, showing both along dip and along strike variations. Creep is observed at the surface along the southern portion of the LVF, where it seems to correlate with Lichi Mélange (Figure 3.1), a formation which has received various debated interpretations (*Biq*, 1971; *Huang and Yin*, 1990; *Huang et al.*, 1992; *Reed et al.*, 1992; *Malavieille et al.*, 2002; *Huang et al.*, 2008; *Wang*, 1976; *Ernst*, 1977; *Page and Suppe*, 1981; *Lin and Chen*, 1986; *Chang et al.*, 2000, 2001, 2009; *Huang et al.*, 2006a).

The objective of this study is to investigate the potential factors that favor aseismic slip on the LVF based on structural and micro-structural analysis of the various formations along the LVF and of rocks from the fault zone. The study is based on field investigations and analysis of samples collected at the outcrop and from drill cores (*Chen*, 2009; *Mu et al.*, 2011). Hereafter, we first describe the different stratigraphic units that compose the Longitudinal Valley area and discuss the nature and origin of the Lichi Mélange. We next discuss its correlation with the creeping section

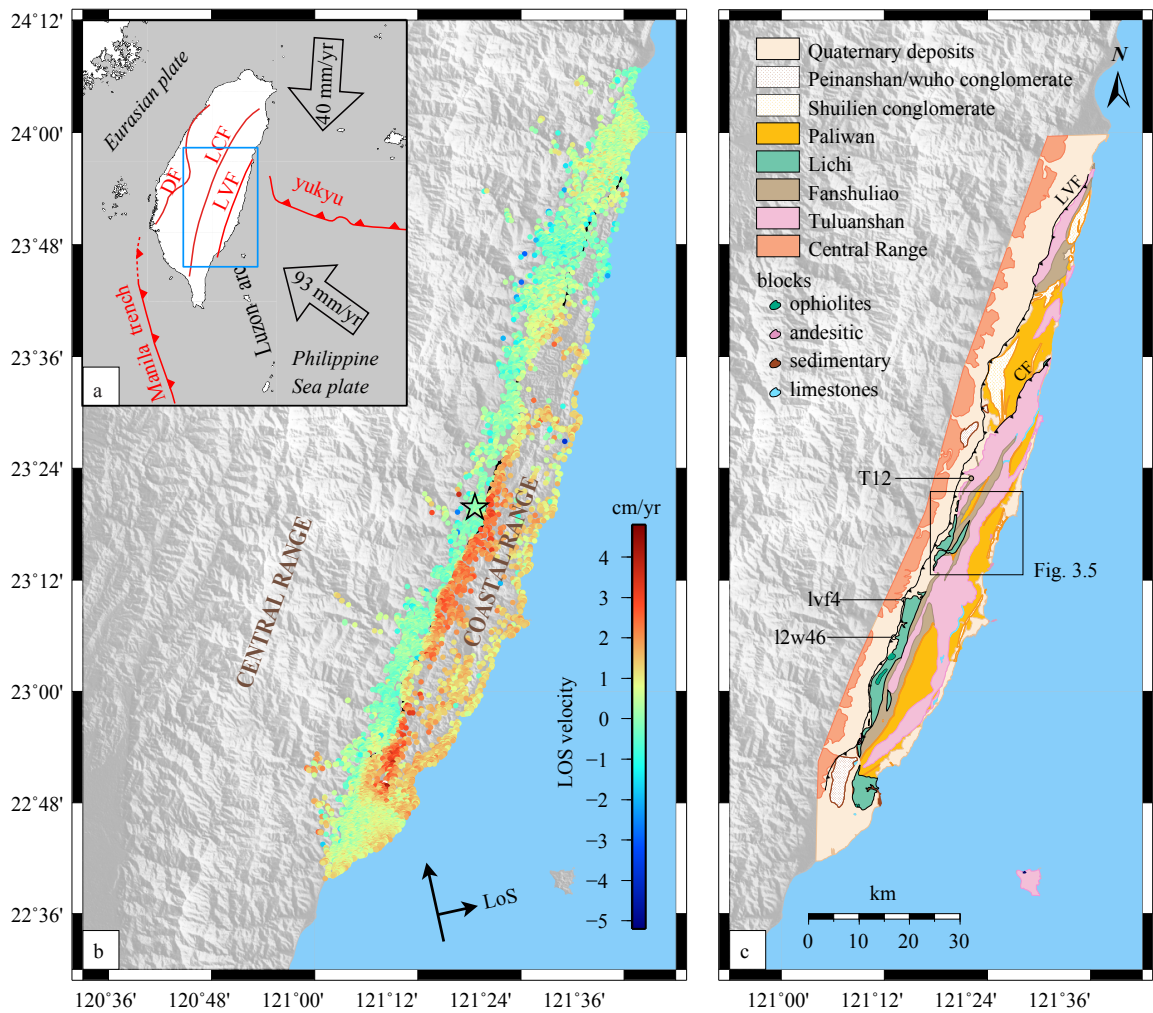


Figure 3.1: (a) Regional tectonic setting of the Longitudinal Valley Fault. The blue rectangle corresponds to the location of subfigure (b). (b) Mean line of sight (LOS) velocity (in cm/yr) around the Longitudinal Valley Fault derived from the Persistent Scatter (PS) technique applied to PALSAR ALOS data acquired between 1/29/2007 and 6/2/2010 (Champenois *et al.*, 2012; Thomas *et al.*, to be submitted). Velocities are expressed relative to the mean velocity of a reference area, indicated by the black star. Black arrows show the ascending track direction and the LOS, which has an incidence of about 35° on average (relative to the vertical). (c) Geological map of eastern Taiwan (modified from Wang and Chen (1993)). The Coastal Range is composed of three accreted Mio-Pliocene volcanic islands (Tuluanshan formation), three remnants of Plio-Pleistocene forearc basins and intra-arc basins (Fanshuliao and Paliwan), and the Pliocene collision Lichi Mélange, which is related to the suturing of the subduction zone due to the collision between the Luzon arc (see subfigure (a)) and the continental margin of South China (Chang *et al.*, 2000, 2001, 2009; Huang *et al.*, 2006a, 2008). Peinanshan and the Wuho are post-collision conglomerates. Central Range formations that border the Longitudinal Valley, include slates and schist Wang and Chen (1993). DF-deformation front; LCF-Lishan-Chaochou Fault; LVF-Longitudinal Valley Fault; CF Chimei Fault.

of the LVF, and we investigate the potential deformation mechanisms which could explain shallow creep on the LVF, based on structural and microstructural observations.

3.2 Stratigraphic and tectonic setting of the Coastal Range

The Coastal Range consists of the Luzon arc volcanic basement and forearc basins, which were accreted to the passive Chinese continental margin during the arc-continent collision, which started about 7 millions years ago (*Liu et al.*, 2000; *Suppe*, 1984; *Huang et al.*, 2006a). We describe here the various rock formations outcropping in their area, their stratigraphic and structural relationships and their mineralogical constituents. This discussion is based on the information available from the literature and our own observations. The location of the sites where observations were carried out and samples collected are indicated in supplemental Figure S1. We conducted two field surveys and collected samples (73 total) for chemical and micro-structural analysis (80 thin sections). We used BSE and SEM to indentify the microstrucrures and X-ray diffraction to characterize the mineralogy. Figure 3.2 shows our revised version of the geological map and sections of the area where most of the field work was focused in order to better constrain the nature and origin of the Lichi Mélange as well as its stratigraphic relationship to the other formations of the Coastal Range.

With regard to the stratigraphy, five rock units can be distinguished in the Coastal Range. The Tuluanshan arc formation, the Fanshuliao volcanoclastic deposits, and the Lichi Mélange are pre-collision island-arc lithofacies, whereas the Paliwan lithic flysch and the Peinanshan and Wuho conglomerates (molasse) are later syn/post-collision lithofacies (Figure 3.1c).

3.2.1 The Tuluanshan arc formation

Stratigraphic and geochemical studies have shown that the Coastal Range is composed of three accreted Miocene-Pliocene volcanic islands, from north to south: Yuehmei, Chimei and Chengkuangao (*Huang et al.*, 2006a, 2008). The volcanic rocks of the Tuluanshan formation represent the former Luzon arc (*Teng and Lo*, 1985). They are distributed all along the Coastal Range (Figure 3.1c) and usually form mountain ridges, covering an area over 1/3 of the Coastal Range. The Tuluanshan formation is considered to be the oldest formation of the Coastal Range. Most of the radiometric dates fall in the range from 23 to 5 Ma with some extending to late Oligocene (29 Ma) and early Pliocene (4.4 Ma) (*Ho*, 1969; *Juang and Bellon*, 1984; *Yang et al.*, 1988; *Chen et al.*, 1990; *Lo et al.*, 1994).

A combined geochronological, geochemical and geophysical study of the Luzon arc has demonstrated that the Luzon arc presents a clear double arc structure related to the eastward shift in volcanism (5-4 Ma ago), most probably due to a change in the dip angle of the slab, which leads to the creation of a new volcanic chain (*Yang et al.*, 1996). As the volcanism in the accreted islands

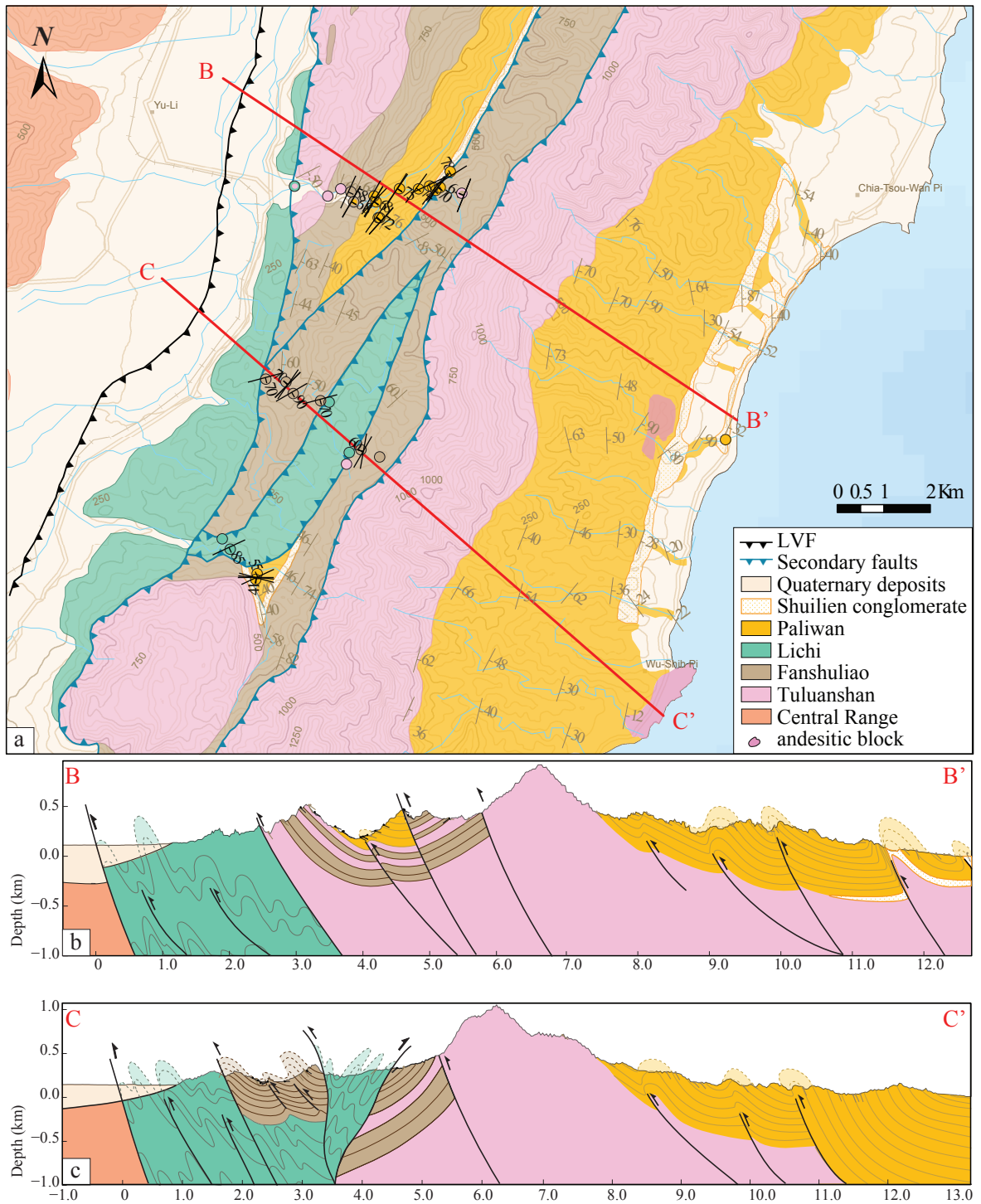


Figure 3.2: Geological map and cross-sections for the central part of the Longitudinal Valley, Taiwan. For location see Figure 3.1. (a) Geological map is modified from Wang and Chen (1993) based on our field observations. Colored-circles show locations of samples. Field-measured dip angles are displayed in black, and measurements from Wang and Chen (1993) are shown in light brown. BB and CC show locations of cross-sections displayed in (b) and (c), respectively. Color coding for the different lithological formations of the Coastal Range are given in (a).

had ceased before then, it is likely that the earlier volcanic centers were, in the early stage of the collision, closer to the trench than the current active volcanic islands. Therefore the three independent islands (Yuehmei, Chimei and Chengkuangao) were not aligned with the present Lutao and Lanshu Islands, south-east of Taiwan.

Volcanic features of the Tuluanshan formation indicate that most were produced by submarine eruptions and a small fraction by subaerial extrusion (*Teng and Lo, 1985*). The following lithofacies have been documented (i) lava, (ii) pyroclastics, and (iii) limestones (*Teng and Lo, 1985; Teng et al., 1988; Chen, 1997a*). A whole spectrum of rocks ranging from basalts, basaltic andesites and andesites can be found, among which andesites are the more voluminous (*Teng and Lo, 1985*). Phenocrysts are generally less than 50 %, of which plagioclase is usually the predominant phase. Hypersthene and pyroxene are inferior to 5 %.

3.2.2 Forearc and intra-arc basins: the Paliwan and the Fanshuliao formations

Three Plio-Pleistocene remnant forearc basins (Shuilien, Loho, Taiyuan) and two intra-arc basins (Chingpu and Chengkung) have been recognized in the Coastal Range (*Huang et al., 2008, 2006a*). Submarine-fan channel deposits, together with paleocurrent measurements (*Teng, 1982; Chen and Wang, 1988*), indicate that the three forearc basins were originally one single basin before the Pliocene arc-continent collision (*Huang et al., 1995*). On the contrary, the Pliocene Chingpu and Pleistocene Chengkung intra-arc basins display no continuity in sediment deposits. They are believed to have developed as a pull apart basin, due to the oblique convergence, on the eastern part of the Neogene Chimei and Chengkuangao volcanic islands, respectively, prior to their accretion on the Coastal Range (*Huang et al., 1995, 2006a*).

Except limestones, most of the sedimentary deposits found in the forearc basin and intra-arc basins display primary sedimentary structures characteristic of turbidites, such as rhythmic alternations of thin persistent sandstone and shale beds, graded beds, sole marks and slump structures. According to the modal composition *Teng (1979)* has distinguished three types of sedimentary rocks, reflecting the variation of sedimentary sources with time. Based on comparison with biostratigraphic studies of the area (*Chang, 1967, 1968, 1969, 1975; Chi et al., 1981*), Type I and II correspond to the so-called Fanshuliao formation, and Type III to the Paliwan formation (Figure 3.1c).

3.2.2.1 Fanshuliao formation

Well exposed in the northern part of the Coastal Range, the Fanshuliao formation conformably overlies the Tuluanshan volcanics with a sometimes interfingering contact (*Teng and Lo, 1985*) (Figure 3.2). The Fanshuliao formation is considered to consist of sediments which accumulated in

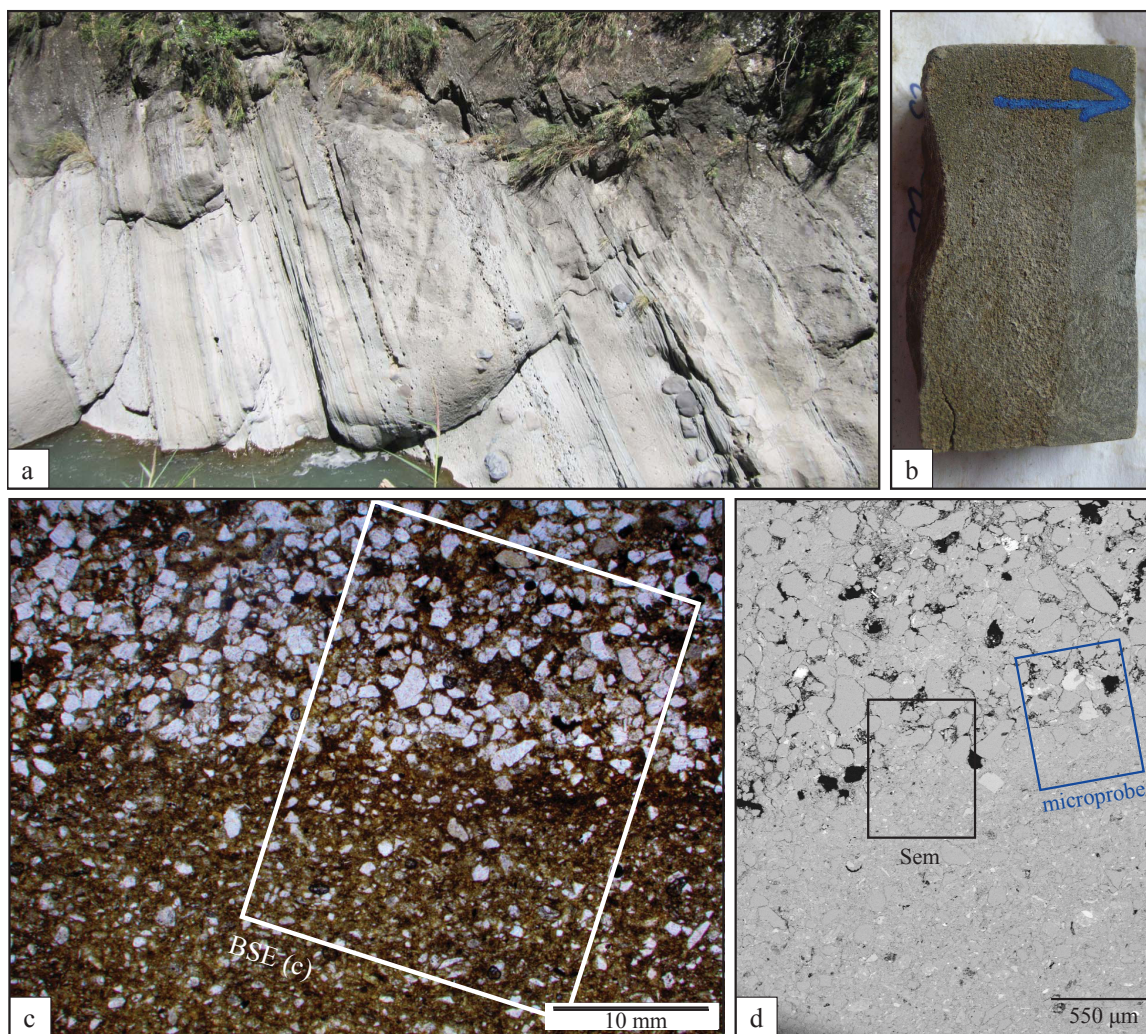


Figure 3.3: Fanchuliao formation. (a) Field view of a Fanchuliao outcrop along the Le-Ho River displaying a typical turbiditic Bouma sequence. (b) T12, a representative Fanchuliao sample collected in the field at longitude $121^{\circ}22'25''\text{E}$ and latitude $23^{\circ}22'55''\text{N}$. See Figure 3.1c for location. (c) Optical micrograph in plane polarized light. Sample exhibits a distinctive layering (s0) with variation in granulometry, characteristics of turbiditic deposits. The white rectangle displays the location of subfigure (d). (d) BSE image from the SEM. Black and blue boxes indicate location of pointshoot X-ray analysis with the SEM (Figure S1 in supplements) and electron probe compositional maps in Figure 3.9, respectively.

the forearc basin between the backstop of the accretionary prism and the Luzon arc islands (*Huang et al.*, 2006b) (Figure 3.6a). Biostratigraphic studies (*Huang*, 1969; *Chang*, 1967, 1968, 1969, 1975; *Chi et al.*, 1981) show that the age of this formation roughly spans the latest Miocene to early Pliocene. Rhythmic alternation of thin sandstone and mudstone beds (Figure 3.3), together with common slump features (meter to hundred meters) are the dominant facies, but characteristic basal mudstone, which represents the draping mud over the volcanic arc in the early Pliocene, can locally be observed. Based on probable source origin, the Fanshuliao formation can be further subdivided into two petrographic types, namely the calcarenaceous volcanoclastic sandstone (Type I) and the quartwacke sandstone (Type II) (*Teng*, 1979; *Teng and Wang*, 1981; *Chen and Wang*, 1988).

In terms of mineralogy content, Type I rocks are marked by a quasi-absence of quartz, a large proportion of volcanic origin feldspar plagioclase (10-40%), the omnipresence of hornblende, some augite and opaques, occasional glauconite and chlorite, and few coalified wood fragments. The epiclastic content of volcanic origin is remarkable (over 50% of the total rock). A large quantity of carbonated bioclasts (20-70% of the total rock) are also found, together with a micritic calcitic cement. Since the mineralogy contents is very similar to the Tuluanshan formation (*Teng and Wang*, 1981; *Chen*, 1997a), arc islands are likely the major source for these sedimentary rocks, transported by turbidity currents to the final depositional basin (*Teng*, 1979, 1980b). Moreover, the lack of terrigenous sediments combined with the abundance of fossil remains lead to the hypothesis of a primary inner, shallow-water shelf environment of deposition, far from the continent.

Unlike in rocks of Type I, quartz is an essential mineral of the quartwacke sandstone (Type II), constituting 10 to 50 % of the total rocks. Nevertheless, plagioclases still dominate, and K-feldspars also occur. With regard to accessory minerals, serpentine is more abundant than hornblende. Augite, chlorite, glauconite and micas can be also found, as well as zircon, tourmaline, garnet and monazite in the heavy fraction. Volcanic fragments are still the prevalent epiclasts, even though the relative quantity of lithic fragments is reduced. Slate fragments occasionally occur in Type II sandstone, and carbonated fossils are still present, but much less abundant than in Type I rocks. Carbonate cement forms an appreciable amount of these sandstones; nonetheless, the detrital clay matrix constitutes 4 to 47 % of the total rock based on the *Teng* (1979) study. Pointshoot X-ray analysis with the SEM is presented in supplementary material (Figure S4).

In the field, Type I and Type II rock units are interbedded, occur evenly and show similar textures. Therefore, they are hardly distinguishable without a petrographic analysis (*Teng*, 1979, 1980b). The main difference is in quartz and fossils content, as well as clay quantity. Consequently, Type II sandstone can be regarded as Type I rocks mixed, to a various extent, with a quartz and alkali feldspar-rich source, likely the non-metamorphic cover sequences of the proto-Taiwan island (*Teng et al.*, 1988) (Figure 3.6b).

3.2.2.2 Paliwan formation

Plio-Pleistocene in age, the Paliwan formation conformably overlies both the Fanshuliao and the Tuluanshan formations (*Teng et al.*, 1988) (Figure 3.1 and 3.2). Grayish in color, this formation includes the whole range of possible facies of deep-sea fan systems and corresponds to Type III sandstones, as described by *Teng* (1979). In terms of mineralogy content, quartz represents 7 to 32 % of the total rock, feldspar is a minor accessory mineral, but serpentine is very common (*Teng*, 1979, 1980b). Detrital grains of pyroxenes are found as well, whereas amphibole is rare. The principal content of those rocks are epiclasts of different origin (14 to 90 % of the total rock) with a relative abundant matrix, composed mainly of pelitic fragments and detrital clays in a smaller amount. Unlike in the Fanshuliao formation, bioclastic grains and calcareous cement are very limited in those rocks (*Teng*, 1979). The dominant type of lithic fragments is basic to ultrabasic igneous rocks, more or less serpentized. Andesitic fragments are rarely present. The other epiclasts are slate and metasandstones (*Teng*, 1979, 1980b), with a progressive decrease through time in sedimentary lithic fragments and an increase first in low-grade and later in medium-grade metamorphic lithic fragments (*Dorsey et al.*, 1988). The voluminous content of strained quartz, slate and metasandstone are undoubtedly derived from a low-grade metamorphic terrain, more likely the exposed Central Range (*Teng*, 1979; *Dorsey et al.*, 1988). The source of the basic rocks is less certain. They might come from the erosion of ophiolite-bearing rock. Finally, the small amount of andesitic epiclasts tells us that the area of deposition was still not far from the arc.

3.2.3 The Lichi Mélange

The Lichi Mélange crops out on the western side of the Coastal Range (Figure 3.1). Its stratigraphic thickness is quite variable and can reach up to ~ 2 km. Biostratigraphic studies (*Chang*, 1967; *Chi et al.*, 1981; *Chi*, 1982; *Barrier and Muller*, 1984; *Huang et al.*, 2008) show a consistent early Pliocene age, which restrains the time of deposition of the protolith to a narrow range (5.5 to 3.7 Ma). Therefore, the Lichi Mélange is coeval with the lower forearc basin sequence but older than the upper deposits of the Paliwan formation.

The Lichi Mélange is a characteristic block-in-matrix mélange with preferred foliation in a scaly argillaceous matrix with slickensided surfaces (Figures 3.4a and b) and boudinage structures in the sandstone blocks (*Chen*, 1997b; *Chang et al.*, 2000). Different sheared facies are observed in the Lichi Mélange: from weakly sheared/broken to highly sheared mélange facies (*Chang et al.*, 2000, 2001; *Huang et al.*, 2008). The weakly sheared, broken formation facies still preserves a distinct turbidite sedimentary structure with a basal layer primarily composed of quartz, like in the lower forearc sequences. However, slate chips, which are commonly found in the upper part of the forearc basin turbidite deposits (< 3 Ma) (*Teng*, 1982), are generally absent in the Lichi Mélange (*Huang*

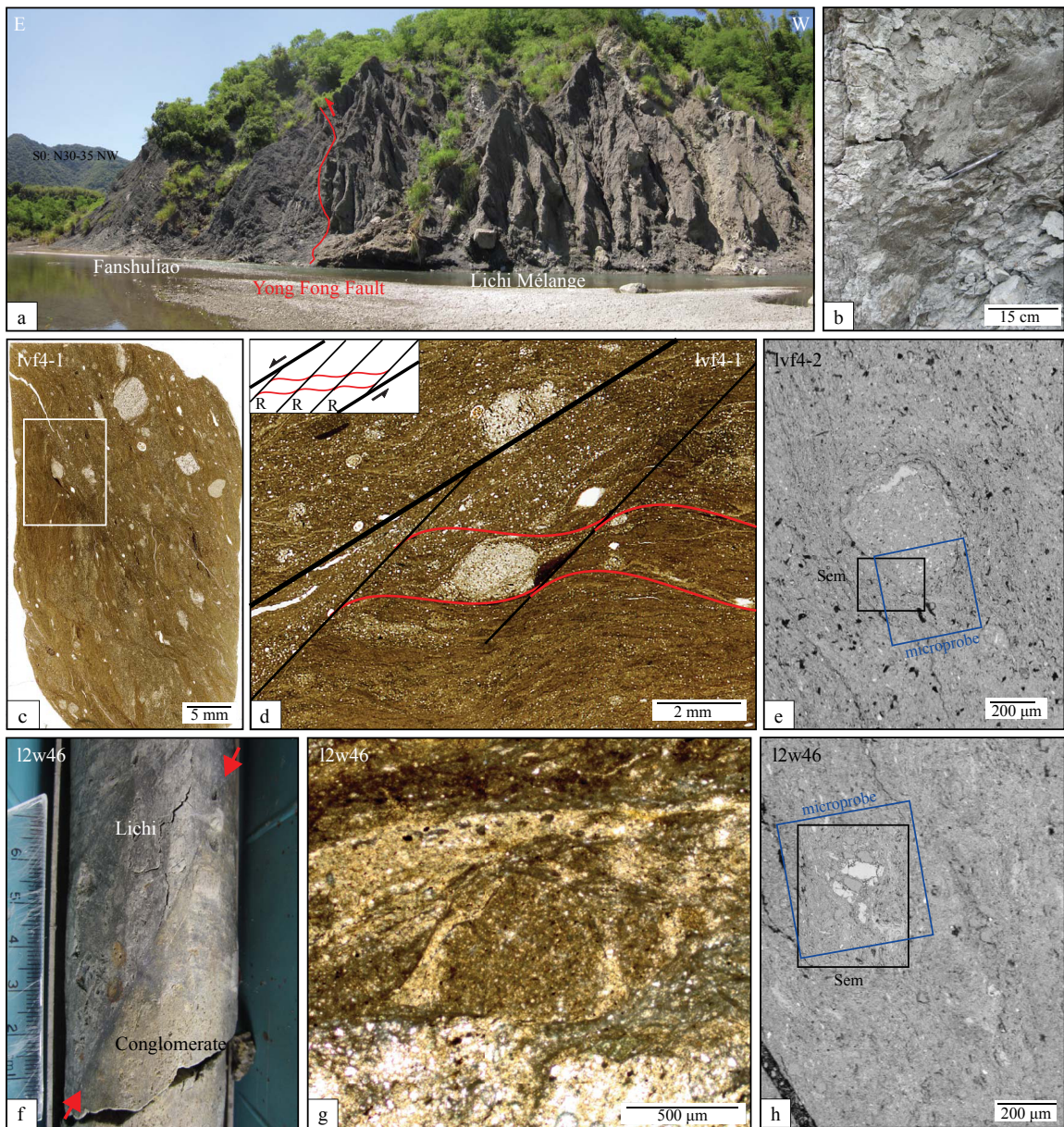


Figure 3.4: Lichi Mélange formation. (a) Contact between the Lichi Mélange and the Fanshuliao formation, near Fuli ($121^{\circ}15'48''\text{E}$ and $23^{\circ}8'35''\text{N}$). The Lichi Mélange is highly erodible and exhibits characteristic v-shape erosion features in the field. (b) Outcrop of Lichi Mélange displaying the typical scaly argillaceous matrix with slickensided surfaces. (c) Thin section of lvf4 sample collected in the field ($121^{\circ}14'32''\text{E}$ and $23^{\circ}9'56''\text{N}$) showing the block-in-matrix structure with penetrative foliation. See Figure 3.1c for location. The white rectangle displays the location of subfigure (d). (d) Typical sigmoid-shaped microstructure with microlithons enmeshed in an clay-rich gouge and oriented along R-type Riedel shear fractures. (f) Borehole core Wan-2 (46.4 m depth along the core section) (Chen, 2009; Mu *et al.*, 2011) displaying the tectonic contact (LVF) between the quaternary conglomerate and the Lichi Mélange. 12w46 samples the main fracture zone highlighted with red arrows. (g) Optical micrograph in transmitted light showing a sigmoid-shaped clast of sandstone. (e) and (h) BSE image from the SEM. Black rectangles indicate the location of the pointshoot X-ray analysis with the SEM (Figure S2 for (e) and S3 for (h) in supplements). Blue boxes correspond to the location of the electron probe compositional maps in Figure 3.7 and 3.8 for (e) and (h), respectively.

et al., 2008).

The exotic blocks inside the formation are of various size (millimeters to kilometers) and lithology (arc products, ophiolites, sedimentary rocks). The volcanic products derived from the Luzon volcanic arc include andesite, volcanic breccias, tuffs and volcanoclastic turbidites. Pillow basalts and gabbro, sometimes serpentinized, composed the dismembered ophiolite suite. The sedimentary blocks show two different facies. One consists of weakly lithified Pliocene turbidite with similar lithology, age and sedimentary turbidite structures as the forearc basin strata (Fanshuliao). The Lichi Mélange also includes metric to kilometric size angular blocks of well-lithified, whitish quartz-rich, feldspathic sandstones, which are late Miocene in age. They have only been observed in the intensely sheared facies of the Lichi Mélange and zircon a fission track study has shown that they are similar to the non-metamorphosed deep-sea fan sandstones of the upper accretionary prism in the Hengchun Peninsula (*Huang et al.*, 1997, 2008). Therefore, those whitish blocks are believed to have been incorporated by eastward thrusting into the deformed forearc strata (*Huang et al.*, 2008).

Clay mineral composition (< 2 m) of the muddy matrix and the sedimentary blocks is similar in all samples, regardless of shearing intensity (*Huang et al.*, 2008). They are characterized by illite, chlorite, mixed-layer clay minerals (mica/smectite) and kaolinite (*Lin and Chen*, 1986) (Figure 3.5 and S2 and S3 in supplements). Smectite alone or serpentine are found as traces or are completely absent. Therefore, the Lichi Mélange must have two sources: one continental with slightly metamorphosed sediments from the exhumed accretionary prism to provide illite and chlorite, and one volcanic to provide the kaolinite. The clay mineral assemblage in the turbidites of the remnant forearc basin is very similar in composition except for the kaolinite, which is absent in the Fanshuliao formation (*Lin and Chen*, 1986). *Huang et al.* (2008) claimed that the occurrence of kaolinite shows the tectonic involvement (thrusting, fragmentation and mixing) of the volcanic basement beneath the forearc basin, during the formation of the Lichi Mélange, with incorporation of the kaolinite from the arc formation by fluid flow along the sheared plan or fractures. Therefore, kaolinite is absent in the forearc basin strata because they did not experience intense deformation.

3.2.4 Stratigraphic relations between the Coastal Range formations

Wherever overlain by the Fanshuliao deposits, the Tuluanshan formation is composed of debris-flow type breccias and turbidites. Moreover, although overlying the arc formation, the Fanshuliao deposits are contemporary to limestones and upper deposits of the Tuluanshan formation (*Teng et al.*, 1988; *Huang et al.*, 1988, 1995). This coevalness suggests that the Tuluanshan limestones and tuffs represent the shallow-water volcanic and fringing reefs environment, and the Fanshuliao turbidites and underlying Tuluanshan debris-flow deposits represent the deep-water deposits in the forearc basin (*Teng and Wang*, 1981; *Teng et al.*, 1988; *Teng and Lo*, 1985; *Chen*, 1997a).

The Paliwan sequences conformably overlie both the Fanshuliao and the Tuluanshan formations

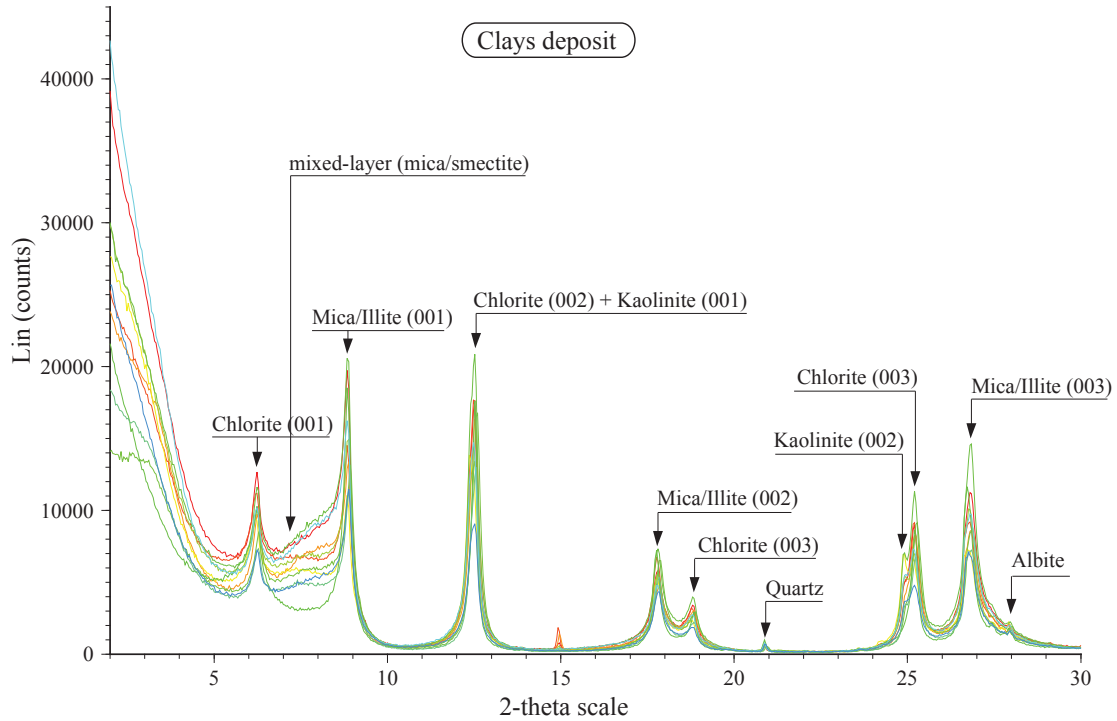


Figure 3.5: X-ray powder diffraction pattern of some oriented clay from Lichi Mélange matrix.

(Figure 3.2). Where it is observed in direct contact with Tuluanshan deposits, the Paliwan formation generally consists of deep-marine mudstones and turbidites resting on either limestones or tuffs (*Teng et al.*, 1988). The facies change associated with this contact is rather drastic and involves significant basin deepening (*Teng et al.*, 1988; *Huang et al.*, 1988, 1995). The contact between the Fanshuliao and the Paliwan formation varies with the facies character of the latter (*Teng et al.*, 1988). While the boundary between the two sequences is a depositional contact in the southern Coastal Range, represented by one layer of pebbly sandstone (*Chen and Wang*, 1988), we clearly observe a sharp, erosional contact in the northern Coastal Range (*Teng and Lo*, 1985; *Chen and Wang*, 1988). Moreover, the formation exhibits overall a southward fining trend, with conglomerates dominating in the north and sandstones in the south (*Teng*, 1982; *Teng et al.*, 1988). These observations lead to the hypothesis of a northern source for the sediments.

The Lichi Mélange is mostly in faulting contact with the coherent forearc basin strata (Fanshuliao, Paliwan) and the Tuluanshan arc formation (*Hsu*, 1956; *Teng and Lo*, 1985) (Figure 3.1 and 3.4b). Nevertheless, depositional contact between the Lichi and Fanshuliao were reported (*Page and Suppe*, 1981; *Barrier and Muller*, 1984; *Huang et al.*, 2008). The Lichi Mélange has been intensely studied, and several origins have been proposed. It was first interpreted as a subduction complex, developed in the former Manila Trench during the subduction of the South China Sea oceanic crust (*Biq*, 1971). But this interpretation is in contradiction to the position of the Lichi

Mélange, which lies east of the accretionary wedge instead of within the accretion prism (*Huang and Yin, 1990; Huang et al., 1992; Reed et al., 1992; Malavieille et al., 2002; Huang et al., 2008*). The Lichi Mélange was later interpreted as an olistostrome (*Wang, 1976; Ernst, 1977; Page and Suppe, 1981; Lin and Chen, 1986*) due to slumping into the western part of the forearc basin of the exposed accretionary prism (proto-Central Range). However, marine seismic investigations in the early 1990s, combined with previous biostratigraphic studies, clays composition and lithology of the exotic blocks inside the mélange, questioned this model and led instead to the proposal of a tectonic collision origin, where the protolith of the mélange is the forearc basin, and the exotic blocks have been incorporated during the early stage of the collision (*Chang et al., 2000, 2001, 2009; Huang et al., 2006a, 2008*). Indeed, the marine seismic profile in the south of Taiwan shows synchronous deformation and sedimentation in the western part of the forearc basin: once the sediments are deposited in the Luzon trough, the sequence is deformed and then covered unconformably by the overlying sequence (*Huang et al., 2008*) (Figures 1.1 and 1.3). On the other hand, in the eastern part of the forearc basin, sedimentation is continuous regardless of active deformation in the west. Near the southern tip of Taiwan, seismic profiles reveal the progressive closure of the forearc basin by arcward thrusting of the forearc basin strata (*Huang et al., 2008; Malavieille et al., 2002; Reed et al., 1992*). The accumulation of deformation and shortening of the forearc basin would have led to the development of the Huatung Ridge, which connects northward with the Lichi Mélange in the southern Coastal Range (*Huang et al., 2008*).

Finally, based on the petrographic features and stratigraphic relations described above, it is likely that the Tuluanshan, the Fanshuliao and the Lichi Mélange formations can be grouped as the pre-collision island-arc lithofacies and the Paliwan formation corresponds to the syn-post collision lithofacies (*Teng, 1979, 1980b*), and, consequently, should instead be considered as a flysch. The effect of this initial collision is well recorded by the deposition of voluminous coarse-grained continent-derived clastics of the Shuilien Conglomerate (Figure 3.1) in the northern Coastal Range (*Teng and Wang, 1981; Teng, 1982*), which started at about 3.5 Ma (*Teng, 1982*).

3.2.5 Tectonic scenario

The mineralogic content and field observations of the stratigraphic relations between the Coastal Range sequences give us clues as to the environment of deposition and tectonic history of the Coastal Range, which allow us to precisely locate the formations with regard to the creeping zone, and the following scenario can be proposed (Figure 3.6):

Intra-Oceanic Subduction

Rifting within the Eurasian continent in the Oligocene (~ 32 Ma) gave rise to the opening of the South China Sea until the Middle Miocene (~ 17 Ma) (*Briaies et al., 1993*). According to radiometric

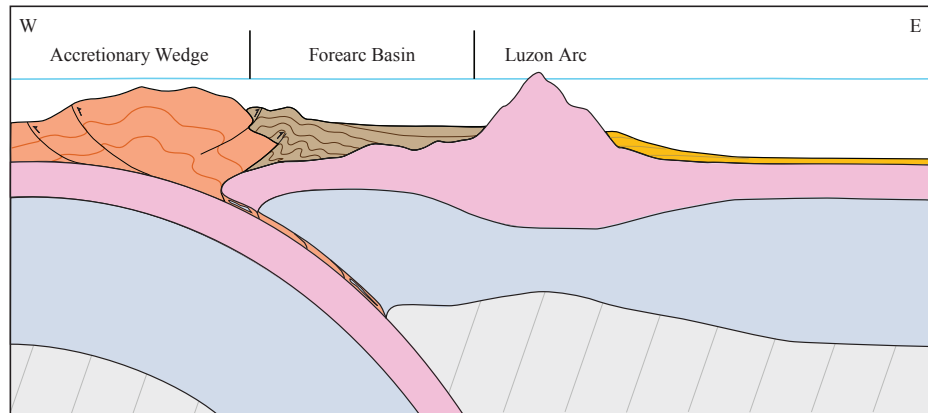
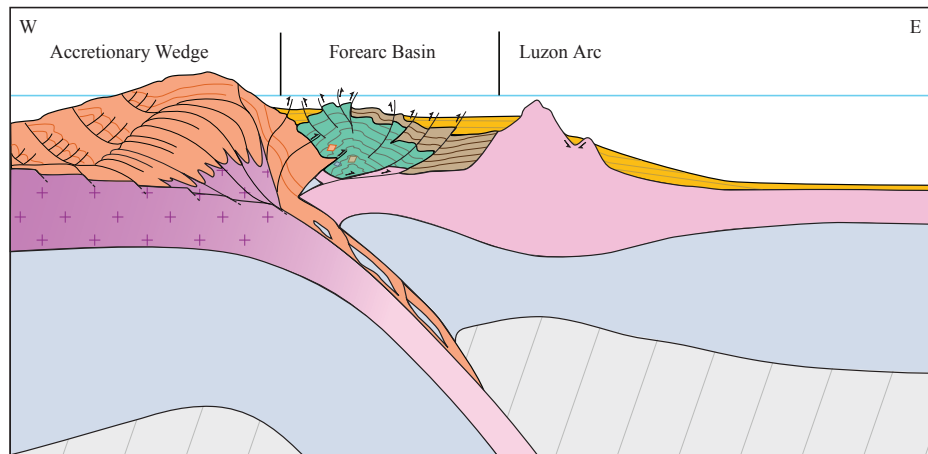
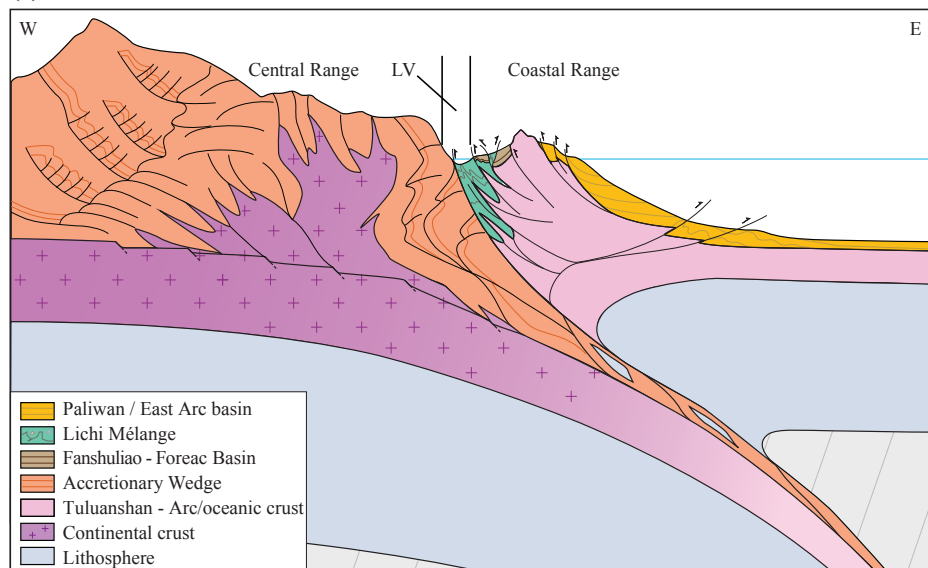
(a) 12 Ma : Intra-Oceanic Subduction Stage (or present south of 21° N)**(b) 5 Ma : Initial Arc-Continent Collision** (or present 22° 2'N)**(c) Present : Advanced Arc-Continent Collision** (or present north of 23° N)

Figure 3.6: Tectonic sketching on the formation of the Coastal Range. (a) Tectonic setting at 12 Ma (or present south of 21°N): intra-oceanic subduction stage. (b) Tectonic setting at 5 Ma (or present 22°2'N): initial arc-continent collision. (c) Current tectonic setting (or present north of 23°N): advanced arc-continent collision.

dating (*Ho, 1969; Juang and Bellon, 1984; Yang et al., 1988; Chen et al., 1990; Lo et al., 1994*), it was quickly followed by the eastward subduction of this basin, beneath the Philippine Sea Plate along the Manila Trench, leading to the creation of the volcanic Luzon arc. From Early Miocene (perhaps late Oligocene) to late Miocene, arc magmatism brought thick sequences of Tuluanshan volcanics and sediment offscraping, filling up the forearc basin (Figure 3.6a). As observed now south of 21°N (profil GMGS973 in Figure 1.3) (*Huang et al., 2008*), once the sediments are deposited in the Luzon trough, the sequence is synchronously deformed and then unconformably overlain by new sequences.

Initial Arc-continent Collision

The initiation of the arc-continent collision starts with the closure of the forearc basin, leading to the formation of the Lichi Mélange (Figure 3.6b). At the same time, as the subduction continues, more and more continental sediments are added in the accretionary prism, which is finally exhumed, providing a new source of deposits for the forearc basin. Cessation of volcanism is also a good marker of the earliest stages of the collision, which suggests a southward propagation : 8-5 Ma for Chimei based on nanofossils (*Chi et al., 1981*) and 3.3 for Chenkuangao based on fission track (*Yang et al., 1988*). Subsequently, fringing reefs start to grow on volcanic islands providing evidences of the termination of volcanism. The oldest Kankgou limestone on the Chimei volcanic island has been dated to 5.2 Ma, and Tungho Limestone (in the south, on the Chengkuangao complex) returned an age of 2.9 Ma (*Huang et al., 1995, 1988*). Based on those observations, it is reasonable to think that the initial arc-continent collision must have begun 7 to 8 Ma ago and that it had already reached 23°5'N at 5.2 Ma (*Liu et al., 2000; Suppe, 1984; Huang et al., 2006b*). The equivalent state is located now at 22°2'N, as observed in seismic profile MW9006-31 in Figure 1.3 (*Huang et al., 2008*). This southward propagation is consistent with the obliquity of the edge of the continental shelf of South China with respect to the subduction zone, which implies a southward migration rate of 90 mm/yr based on *Suppe (1984)* or 60 mm/yr based on *Byrne and Liu (2002)*. (*Dorsey et al., 1988*) study of the subsidence and uplift of the basins in the Coastal Range also concluded a migration rate of about 60 mm/yr.

Advanced Arc-Continent Collision

The westward thrusting and accretion of the Luzon arc and forearc sequences onto the Asian continent, conjointly with the exhumation of metamorphic basement in the Central Range, mark the final stage of the arc-continent collision (Figure 3.6c). This stage should be younger than the youngest strata found on the forearc basin sequences. Bio- and magnetostratigraphic studies (*Chang, 1975; Chi et al., 1981; Hornig and Shea, 1997; Lee et al., 1991*) indicate that Coastal Range formations must have been accreted roughly 1.5 Ma ago in the north and 1.1 Ma in the south (*Huang et al.,*

2006b).

3.2.6 Origin of latitudinal variations in the occurrence of the Lichi Mélange

The Lichi Mélange is thus interpreted as the result of the deformation of the forearc strata and basement in the early stage of the collision. One might then wonder why there is almost no occurrence of the Lichi Mélange in the northern half of the Coastal Range.

The southward propagation of the arc-continent collision in Taiwan, as well as the indication that the volcanic activity within the Luzon arc shifted eastwards (*Yang et al.*, 1996) can today, south of Taiwan. Moreover, we should consider an increase over time of sediment supply in the forearc basin, with the exhumation of the accretionary prism and the continental basement. Consequently, a southward decrease of the thickness of the forearc basin sequences as well as a decrease in lithic content should be expected. Hence, the extent of the Lichi Mélange formation should be reduced northward.

Additionally, the northern termination of the Lichi Mélange outcrops correlates with a major tectonic feature of the Coastal Range, the Chimei Fault (Figure 3.1b and c), which splits the Coastal Range into northern and southern blocks. It is a left-lateral reverse fault with N-S compression, which separates the Tuluanshan and the Paliwan formations (Figure 3.1c) and which is ascribed a total offset of up to several kilometers (*Chen et al.*, 1991; *Kuo*, 2013). Therefore, the Chimei fault, and a probable northward decrease in thickness of the Lichi Mélange formation, might explain the rather abrupt termination of the Lichi Mélange outcrops.

Finally, it is also possible that the highly erodible Lichi Mélange would have been eroded away thanks to the thrusting component and the high erosion rate estimated to be more than 10 mm/yr in the Coastal Range (*Dadson et al.*, 2003). Therefore, the few spotty outcrops of potentially Lichi Mélange reported to the north of the Chimei Fault (Figure 3.1c) (*Teng*, 1980a) may well be the remnants of the Lichi formation, which was squeezed out upon land in the early stage of the collision.

3.3 Deformation mechanisms in the Lichi Mélange

3.3.1 Spatial correlation of aseismic slip with the Lichi Mélange

As mentioned in the introduction, the southern half of the LVF is clearly creeping at the surface. The lateral extent of the creeping segment is well revealed by the map of mean LOS velocity (in cm/yr) derived from the Permanent Scatter technique applied to PALSAR ALOS data acquired between 01/12/2007 and 09/07/2010 (*Champenois et al.*, 2012; *Thomas et al.*, to be submitted) (Figure 3.1b). This map shows a clear step in the LoS velocity field (positive toward the satellite) along the LVF,

south of $23^{\circ}30'$. The discontinuity is clear evidence of aseismic slip near the surface for the southern portion of the LVF, and comparison with surface geology supports earlier inferences (*Hsu et al.*, 2009a) that the Lichi Mélange would be responsible for promoting aseismic creep (Figure 3.1). By contrast, no clear discontinuity (at the detection level of the technique, estimated to be ~ 2 mm/yr at the 67% confidence level) is observed along the northern half of the LVF, suggesting that the shallow portion of the fault has remained locked over the 2007-2010 period. The lack of aseismic slip correlates with the disappearance of the collision mélange since only isolated outcrops of the Lichi Mélange have been recognized north of the Chimei Fault (*Teng*, 1980a) (Figure 3.1c). Therefore, in the particular case of the LVF, lithology seems to control the along strike variations of slip mode. We now examine the potential mechanisms which could explain enhanced aseismic creep where the fault is bounded by the Lichi Mélange. We examine in particular the difference of structure and mineralogical composition between the Lichi Mélange and the forearc formations.

3.3.2 Selection of field and core samples

Two field surveys and one core sampling have been conducted to study the different units of the Coastal Range. A total of 59 samples from the Lichi Mélange, Fanshuliao, Tuluanshan and Pailwan outcrops were collected, and 63 thin sections were prepared and analyzed (see Figure S1 in supplementary materials for location). We also sampled cores from shallow drillings, which were conducted near Chihshang ($121^{\circ}22'E$, $23^{\circ}10'N$) (*Chen*, 2009; *Mu et al.*, 2011). We collected samples from the fault zone, as expressed by the intense macroscopic fracturation and foliation: 14 samples from the Wanan sites (Wan-1 and Wan-2) were selected, and the analysis of 16 thin sections has been carried out. All petrographic sections were polished sections to allow both optical and electron microscopy. Samples containing Lichi Mélange were impregnated with clear epoxy resin before cutting. We first resorted to optical transmitted and polarized light microscopy to examine the mineralogy contents and microstructures. A total of 11 field samples were also selected to perform a clay mineral analysis of the Lichi Mélange (Figure 3.5). High-resolution SEM combined with Energy-dispersive X-ray spectroscopy (EDS), as well as electron probe micro-analyzer were used for imaging the fault rock microstructures and determining the mineral phases of the Lichi samples from the fault zone (Figures 3.9, 3.7, 3.8 and S2, S3, S4 in supplementary materials). The selection of samples was based on microscopy analysis.

Hereafter we describe three representative samples for describing the LVF: (1) lvf4, a Lichi Mélange sample collected in the field ($121^{\circ}14'32''E$ and $23^{\circ}9'56''N$) on the LVF (Figure 3.4c-d), (2) l2w46, a sample from the borehole core Wan-2 at 46.4 m depth along the core section (*Chen*, 2009; *Mu et al.*, 2011), displaying the tectonic contact (LVF) between the quaternary conglomerate and the Lichi Mélange (Figure 3.4f-h) and (3) T12, a typical Fanshuliao sample collected in the field at longitude $121^{\circ}22'25''E$ and latitude $23^{\circ}22'55''N$, as a protolith reference for the Lichi formation

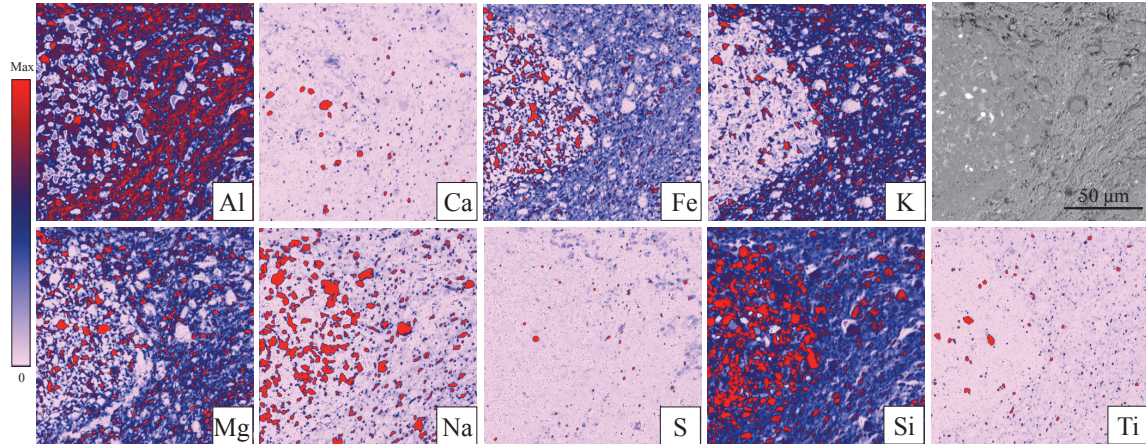


Figure 3.7: Electron probe micro-analyzer compositional maps of sample Lvf4, displaying a microlithon enmeshed in foliated matrix. The Lichi Mélange sample was collected in the field, inside the LVF fault gouge (Figure 3.1c). For location of the analysis, see Figure 3.4e. Red, blue and white colors indicates high, intermediate and missing contents respectively. The distribution of Aluminium indicates pervasive clay mineralization of the foliated matrix. The foliated gouge is also clearly depleted in Si, Ca and Na and passively concentrated in K, Al, Fe, Mg, Ti, and S compared to the microlithon (initial state), showing a deficit in soluble minerals that is likely related to pressure-solution diffusive mass transfer. The top-right corner figure is the corresponding BSE image of the area.

(Figure 3.3). See Figure 3.1c for the location of those three samples .

3.3.3 Microstructural and analytical observations

The fault gouge in the Lichi Mélange consists of altered, highly comminuted, scaly foliated rocks with slickensided surfaces and striations. All samples are pervasively sheared and display a characteristic anastomosing phyllosilicates foliation with sigmoidal microlithons and strain shadows (Figures 3.4d and c) that define R-type Riedel shear surface (*Rutter, 1986*). They provide a clear indication of bulk ductile flow. Foliation is defined by millimetric to sub-millimetric alternation of clay and quartz-rich bands (Figures 3.4a and b) that contain microstructural evidences of reworked cataclasites as well as mineralogic differentiation, which are likely related to pressure solution mass transfer (Figures 3.7 and 3.8). Pyrite minerals in the gouge provide evidence for hydrothermal fluid flow (Figures 3.8 and S2 in supplementary materials). Blocks in the matrix can be sub-millimetric to kilometeric in size. In the thin sections we analysed they mostly consist of quartz-rich or calcite-rich lithic fragments with micro-fossils. Most remarkably, there are no veins in the gouge. By contrast, sandstone blocks in the foliated matrix are pervasively fractured with open fractures filled with calcite or breccias cemented by calcite (*Chen, 1997b*), which appear to have been injected, presumably under high fluid pressures.

The textural differences between the Fanshuliao formation (protolith equivalent) and the Lichi Mélange are emphasized by the electron probe micro-analyzer compositional maps presented in

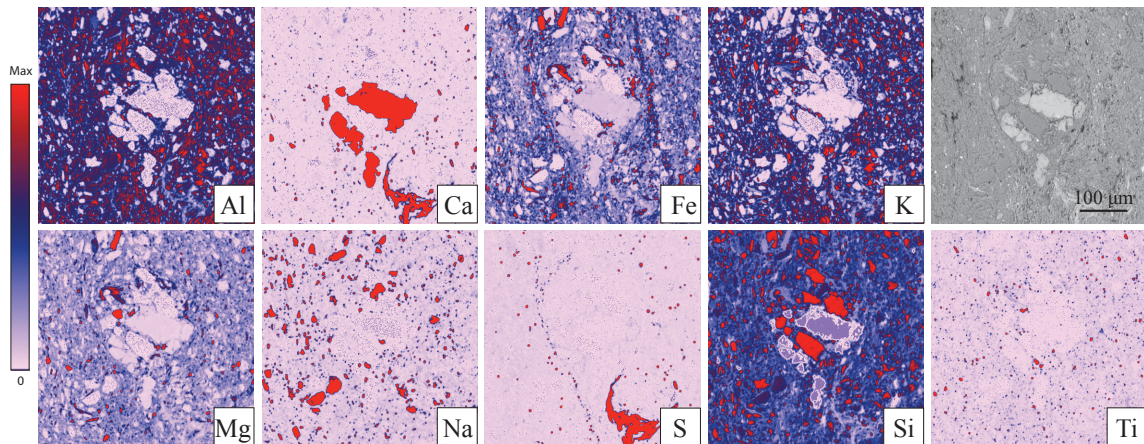


Figure 3.8: Electron probe micro-analyzer compositional maps of sample L2w46, displaying a sigmoidal microlithon embedded in foliated matrix. L2w46 was sampled on the borehole core Wan-2 at 46.4 m depth along the core section (Figure 3.1c). For the location of the analysis, see Figure 3.4h. Red, blue and white colors indicate high, intermediate and missing contents respectively. Distribution of Aluminium indicates pervasive clay mineralization of the foliated matrix. The foliated gouge is also clearly depleted in Si, Ca and Na, and passively concentrated in K, Al, Fe, Mg, Ti and S compared to the microlithon (initial state), showing a deficit in soluble minerals that is likely related to pressure-solution diffusive mass transfer. Evidence of pyrite masses in the gouge also favours the presence of hydrothermal fluid flow. The top-right corner figure is the corresponding BSE image of the area.

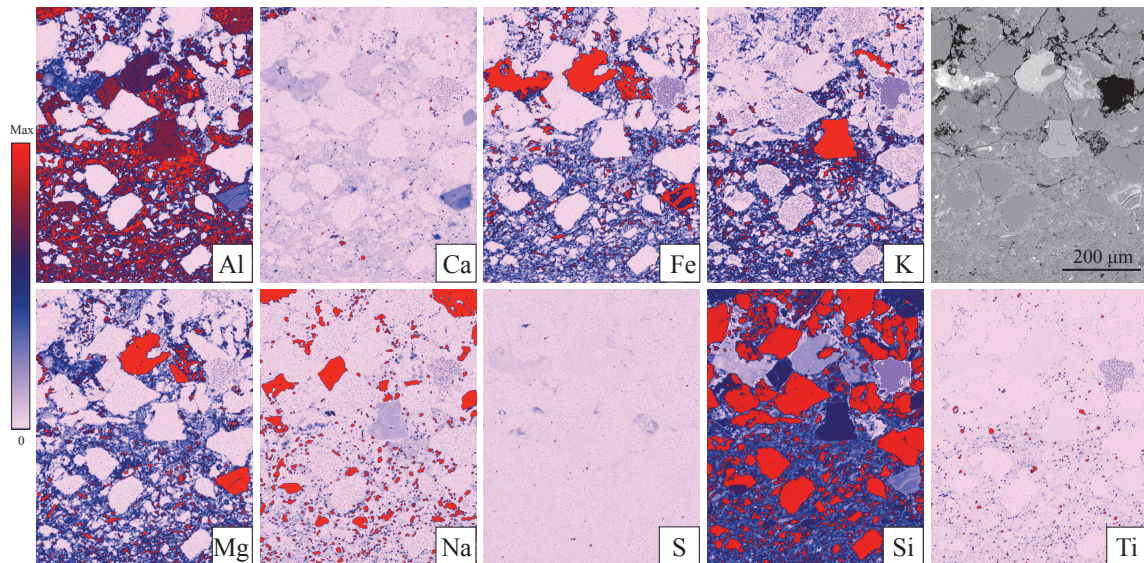


Figure 3.9: Electron probe micro-analyzer compositional maps of one typical forearc-basin formation sample (Fanshuliao) showing that no substantial differentiation is observed in the two sedimentary layers, which seems to display the same mineralogical contents (a slight increase in Ti may be inherited). The only difference stands in the grain size. For the location of the analysis, see Figure 3.3d. The top-right corner figure is the corresponding BSE image of the area, and red, blue and white colors in the compositional map indicate high, intermediate and missing contents, respectively.

Figures 3.7, 3.8 and 3.9. The fault gouge, compared to sample T12 or the microlithons, which represent an initial state of the Lichi Mélange, is dominated by the development of a very fine grain matrix and foliation seams with a depletion of Si Ca and Na and a passive concentration of K, Al, Fe Mg, S, Ti. This corresponds to the dissolution of soluble minerals, such as quartz, feldspars and calcite, and the passive concentration of phyllosilicates and titano-ferro oxides associated with a possible recrystallization of the phyllosilicates. Quartz, calcite and feldspar are, on the contrary, preserved inside the microlithons and in the strain shadows of those grains (Figures 3.7 and 3.8).

3.4 Discussion

3.4.1 Deformation mechanisms of the Lichi Mélange and control on the aseismic behavior of the LVF

The microstructural study of the fault zone samples shows that the deformation on the LVF is accommodated by grain boundary sliding. Such a deformation mechanism can be operated by frictional sliding (with granular and/or cataclastic flows) or pressure-solution creep. The deformation observed in those fault zone rocks reflects the cumulative tectonic history since the onset of deformation of the Luzon forearc. The exhumed fault zone does not show much evidence for metamorphism, consistent with the low exhumation (less than 2km) (*Shyu et al.*, 2006) and relative cold conditions (Temperature less than 450°C in the 0-30 km depth range) inferred from the thermokinematic modeling of *Simoes et al.* (2007a). Note, however, that the estimated thermal structure is not well calibrated for the Coastal Range due to the lack of thermobarometric and thermochronological constraints in this area. However, it is likely that the deformation observed in the exhumed fault zone is representative of the ongoing deformation on the LVF at a relatively shallow depth (a few kilometers).

The primary fault zone processes observed in this study are the strong reduction of grain size and the pervasive foliation. Several processes might lead to grain-size reduction that include cataclasis, stress corrosion, dynamic recrystallization and neomineralization (*Snoke et al.*, 1998). The Lichi Mélange sample show evidence of cataclastic flow, which has been interpreted to be related to the early deformation of the forearc basin strata, based on the cross-cutting relation with the foliation (*Chen*, 1997b) (see section 3.2.4). On the other hand, the development of a strong anastomosing foliation inside the Lichi Mélange, the presence of sigmoidal porphyroclasts and microlithons and the evidence of strain shadows (Figures 3.4, 3.7 and 3.8) demonstrate the dominant role of pressure solution creep. Stress-driven dissolution is also strongly supported by the depletion in Ca-Na feldspar, quartz and calcite in the foliated matrix, whereas we observe an enrichment in phyllosilicates and oxides (Figures 3.7 and 3.8). There is no evidence of redeposition in veins nearby; however, soluble species may have been transported away from the zone of dissolution and such fluid flow may likely

be the source of the hydro-fracturing observed in sandstone blocks (*Chen, 1997b*).

Evidences of pressure-solution creep do not exclude the fact that part of the creep is accommodated by granular flows, involving friction. R-type Riedel slip surfaces in the clay-rich matrix surround the microlithons (Figure 3.4d) and demonstrate intrinsic material weakness. Aseismic slip might also occur by a granular flow mechanism that involves frictional sliding of microlithons in a matrix of phyllosilicates.

3.4.2 Influence of mineral frictional properties on fault slip mode

The matrix of the Lichi Mélange is rich in illite, chlorite, mixed-layer clay minerals (mica/smectite), which are also common constituents of subduction mélanges. Illite has long been thought to be dominantly velocity-weakening and smectite velocity-strengthening. The illitization of subducted sediments (smectite transforms to illite when the temperature get higher than about 450°C) was then considered to be the possible mechanism responsible for the updip limit of the seismogenic zone (*Hyndman et al., 1997*). Recent experimental work has shown that the illite clay gouge is actually velocity-strengthening in the 0 – 250°C temperature range (*Saffer and Marone, 2003; Saffer et al., 2012; den Hartog et al., 2012b,a*). In fact, experimental studies show that, overall, unconsolidated and unlithified clay-rich gouges promote a velocity-strengthening behavior, and hence aseismic deformation, independently of their composition (in particular, the smectite/illite ratio) (*Rutter and Maddock, 1992; Saffer and Marone, 2003; Ikari et al., 2009; Saffer et al., 2012*). This result is consistent with the observation that the Lichi Mélange promotes aseismic slip at shallow depth on the LVF.

However, most intriguingly, there is no key mineralogical difference between the matrix of the Lichi Mélange along the creeping segment in the South and the forearc formations along the locked segment in the north. They only differ in the presence of kaolinite (see subsection 3.2.3), which displays both velocity-strengthening and velocity-weakening behavior at a low slip rate (11 $\mu\text{m/s}$), relatively low normal stress ($\sigma = 20 - 50$ MPa), and a high frictional strength ($f_o = 0.6$) (*Ikari et al., 2011a*). In agreement with previous mineralogic studies (*Lin and Chen, 1986*) we did not find evidence for talc, serpentine or saponite (a form of smectite), which have been advocated to account for the aseismic creep on the San Andreas fault (e.g. *Solum et al., 2006; Morrow et al., 2007; Moore and Rymer, 2007; Lockner et al., 2011; Carpenter et al., 2011*). Therefore, it seems unlikely that the inherent frictional properties of the fault zone mineral constituents can explain why aseismic creep is favored at shallow depth on the southern segment of the LVF.

Nevertheless, the development of the foliation itself, as a microstructural weakening mechanism, could have substantially altered the mechanical properties of the Lichi Mélange compared to its undeformed protolith. The development of the foliation indeed favors low friction minerals, which, even though they might represent a very low mass fraction of the constituents, can turn out to

dominate the mechanical properties of a fault zone (*Collettini et al.*, 2009; *Niemeijer et al.*, 2010a; *Ikari et al.*, 2011b). Besides, *Ikari et al.* (2011a) have found a systematic relationship between absolute frictional strength and the potential for unstable fault slip. Weak gouges, with coefficients of friction $\mu < 0.5$, exhibit only stable sliding behavior, whereas strong gouges, with $\mu \geq 0.5$, exhibit both stable and unstable slip (*Ikari et al.*, 2011a). Accordingly, even with similar mineralogic content, the well-foliated Lichi Mélange is more likely to display a velocity-strengthening behavior than the forearc basin strata that preserved the bedding structure.

3.4.3 Can pressure solution creep explain the lithological control of aseismic slip on the LVF?

The discussion above shows that the deformation of the Lichi Mélange along the LVF has involved pressure solution creep. For pressure-solution creep to develop and accommodate large creep rate, specific conditions are required. Soluble minerals such as quartz, calcite or feldspar, which have been proved to be abundant in the Lichi Mélange, must be present and interact with a fluid phase. Note that the solubility of these minerals varies with the temperature: calcite is more soluble at low temperature, whereas the dissolution of quartz and feldspar is more efficient at high temperature. Here we see on the outcrop the cumulative effect of this process since the Litchi Mélange, which is now at the surface, was dragged from depth along the thrust zone.

The rate of pressure solution creep is known to be inversely proportional to the cube of the grain size (*Rutter*, 1976). Therefore, very fine grained material decreases the distance of diffusive mass transfer and consequently increases the efficiency of the deformation mechanism (*Twiss and Moores*, 1992; *Gratier et al.*, 2011, 2013). Finally, the enhancement of pressure-solution creep under the influence of phyllosilicates has been recognized (*Weyl*, 1959; *Renard et al.*, 1997): clay minerals provide higher diffusivity in the contact layer and prevent the sealing of grains, which keep fast diffusive paths along solution seams (*Niemeijer and Spiers*, 2005; *Gratier et al.*, 2011). Therefore, the Lichi Mélange, compared to others lithological formations in the Coastal Range, gathers the specific conditions for pressure solution creep to exist, to persist in time and to accommodate large strain rates.

Pressure-solution creep has been shown to be a key factor in promoting aseismic deformation of synthetic fault gouge (*Niemeijer et al.*, 2010b). This experimental study demonstrates that pressure-solution creep tends to inhibit the strain-weakening behavior associated with pure mechanical deformation of the fault gouge. We suspect that such a mechanism could explain the large fraction of aseismic slip on the LVF. One objection to pressure-solution creep being the rate-controlling factor is that this mechanism predicts a linear viscous flow law (*Rutter*, 1976), while postseismic aseismic creep is highly non-linear in general, as was observed on the LVF, following

the 2003 Chengkung Earthquake on the LVF (*Thomas et al.*, to be submitted; *Hsu et al.*, 2009b; *Chang et al.*, 2009). The abrupt acceleration of creep and the typical $1/t$ decay of afterslip rate following that earthquake is consistent with the behavior predicted by velocity-strengthening frictional sliding (*Marone et al.*, 1991; *Perfettini and Avouac*, 2004). However, it should be pointed out that velocity-strengthening friction is a phenomenological behavior that could result from a variety of different deformation mechanisms. Pressure-solution creep could actually be involved. *Gratier et al.* (2009) and *Gratier* (2011) have indeed demonstrated that micro-fractures development can drastically accelerate pressure solution creep rate: fracturing reduces the diffusive mass transfer distance, which is the rate-limiting effect. However, if the fractures are progressively sealed, this effect disappears and consequently reduces the displacement rate and shows exponential decrease (*Gratier et al.*, 2009). Such a mechanism would allow for reconciling the evidence for pressure-solution creep with the the acceleration of creep observed after the 2003 Chenkung earthquake and the later decay of afterslip rate.

Note that evidence of slickensides in the Lichi attest to cataclastic processes that must contribute to the creeping process. As the sliding occurs on relatively high friction minerals (see section 3.4.2) it must be associated with an increase in temperature. The partition between mass transfer through pressure-solution creep and friction process could be inferred, in theory, by measuring the temperature inside the creeping zone. This remains to be done, and it is not an easy process, due to the possible artifact effect of fluid cooling.

3.5 Conclusion

Based on the kinematic study of the LVF (*Thomas et al.*, to be submitted) and the tectonic analysis of the Coastal Range formations, we conclude that there is a strong lithological control of the mode of slip on the LVF: the presence of the Lichi Mélange clearly promotes aseismic creep. This finding is consistent with experimental studies which have demonstrated the velocity-strengthening behavior of clay-rich gouges at low ($T < 250^\circ\text{C}$) temperatures (*den Hartog et al.*, 2012a; *Saffer et al.*, 2012).

The lithological, meso- and microstructural evidences from the fault core samples suggest that it is likely that both frictional sliding (by cataclasis or granular flow) and pressure-solution creep concur to accommodate grain boundary sliding within the LVF gouge. A similar mode of deformation has been observed in experimental deformation of synthetic gouge (*Niemeijer et al.*, 2010b). Presumably, in such a context of competing deformation mechanisms, the less energy-consuming process should dominate (*Beeler et al.*, 1996). We argue that that pressure-solution creep is probably determining the creep rate, as in the experimental study, due to favorable conditions for pressure-solution creep inside the Lichi Mélange. As long as soluble minerals are present in the fault gouge, and those soluble species are transported away from the zone of dissolution, preventing restrengthen-

ening mechanisms such as cementation or fracture sealing, pressure-solution creep should be the dominating deformation mechanism. It is an efficient mechanism to accommodate aseismic creep through the entire upper crust down to more than 10 km (*Gratier et al.*, 2011). Episodic particle size reduction by cataclasis and alteration of feldspars to phyllosilicates are processes that would assist the pressure-solution creep mechanism and are likely to occur in the Lichi Mélange. The partition between dissolution and friction processes, which accommodate the sliding of the mineral elements, could be evaluated by measuring the temperature of the creeping zone, but this remains to be done.

This study suggests that aseismic creep is probably favored in the presence of any non-lithified subduction mélange, and that the internal structure of a fault gouge, namely the foliation, comminuted grain sizes, and the mixing of soluble and insoluble minerals, is more important in determining the mechanical properties of the fault zone than the mechanical properties of its mineral constituents, adding support to the view that fault zone fabric is essential in explaining fault mechanical properties (*Collettini et al.*, 2009; *Niemeijer et al.*, 2010a; *Ikari et al.*, 2011b).

Lithological control on the spatial evolution of fault slip
on the Longitudinal Valley Fault, Taiwan -
Supplementary materials

July 23, 2013

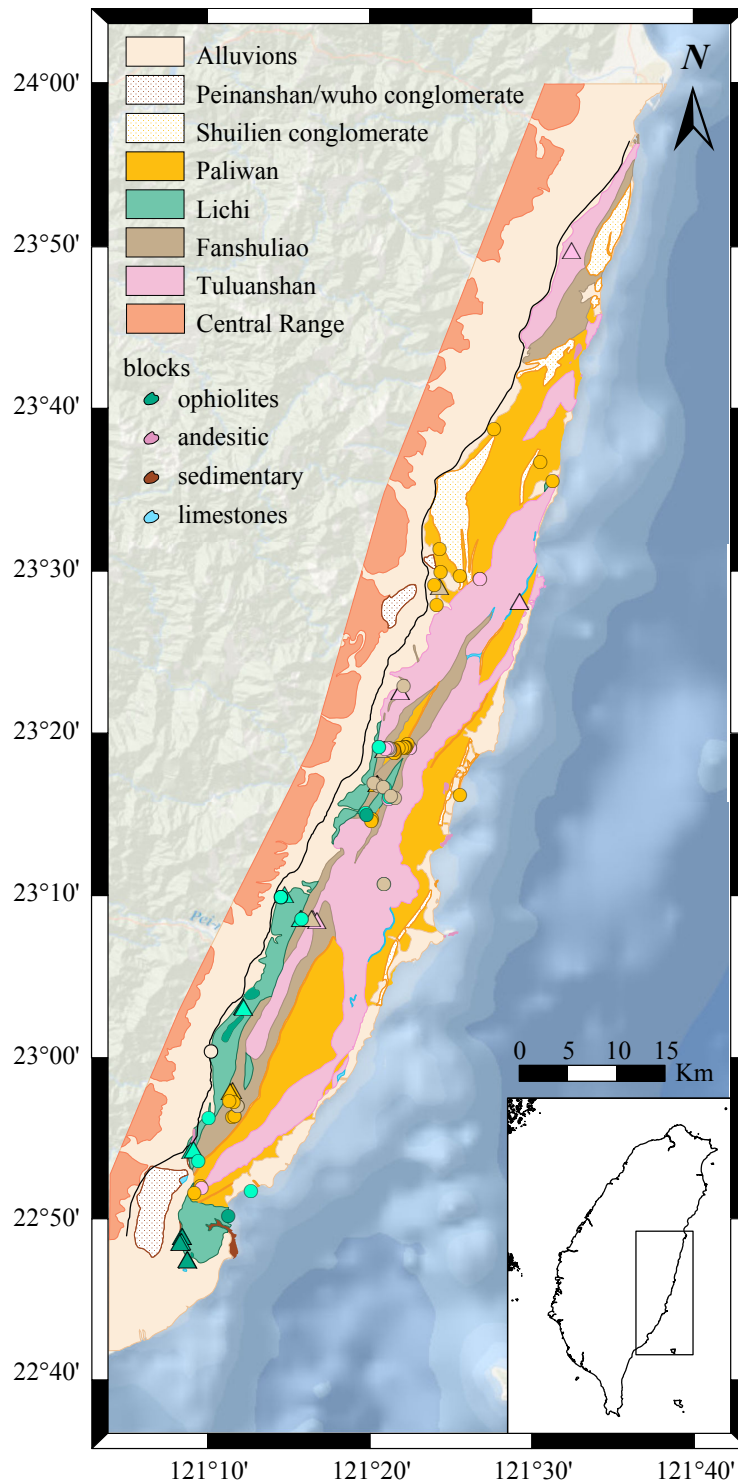


Figure S1: Geological map of eastern Taiwan (modified from Y. Wang and W.S Chen, 1993) and locations of samples collected in the field. Circle are samples collected in September 2012 while triangles gives the locations for the April 2010 sampling survey. Color attributions for samples and Lithological formations are identical.

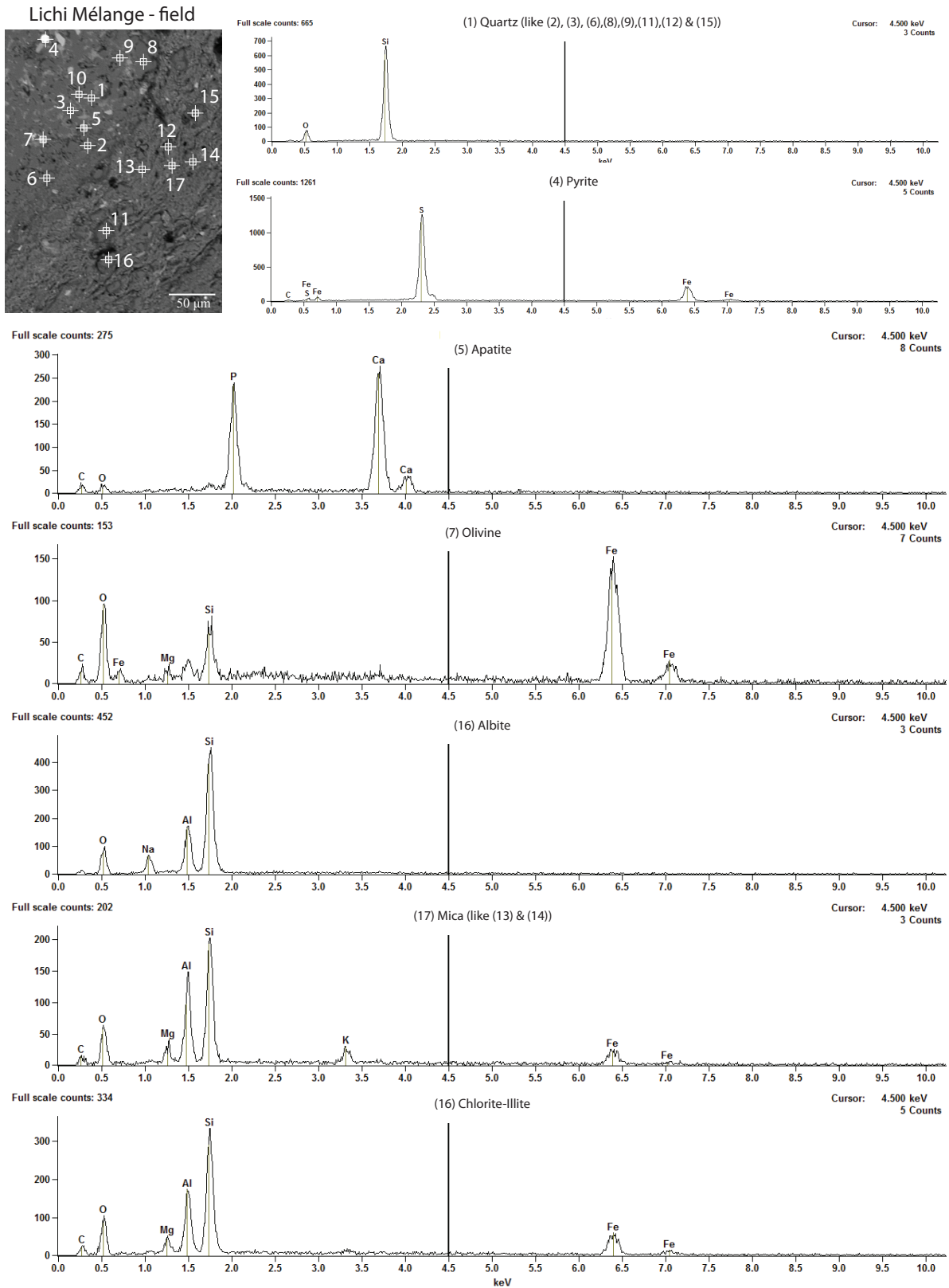


Figure S2: Representative EDS traces of grains inside de fault gouge, sample lvf4 (Lichi Mélange). For location of the analysis, see Figure 3.3e.

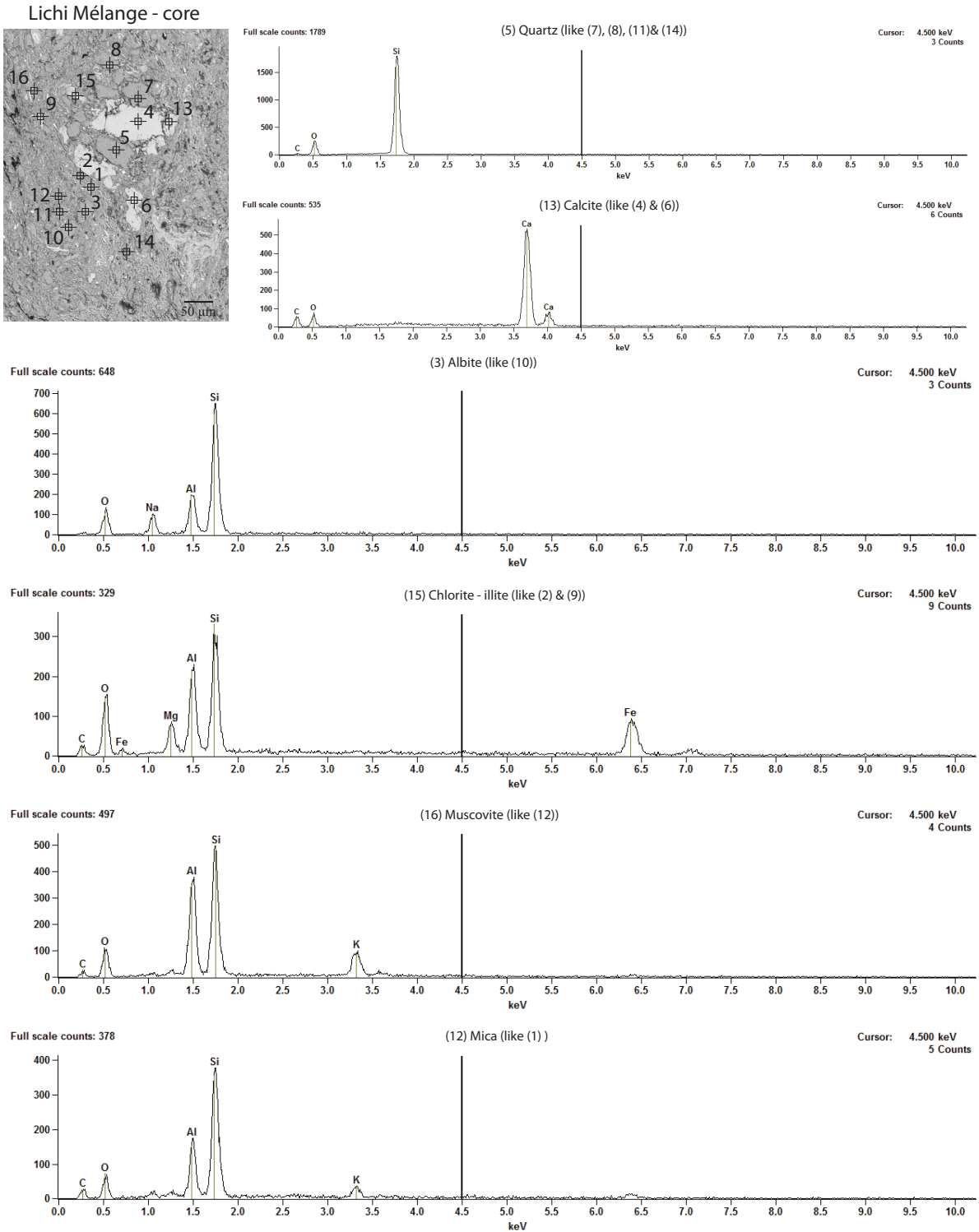


Figure S3: Representative EDS traces of grains inside de fault gouge, sample 12w46 (Lichi Mélange). For location of the analysis, see Figure 3.3h

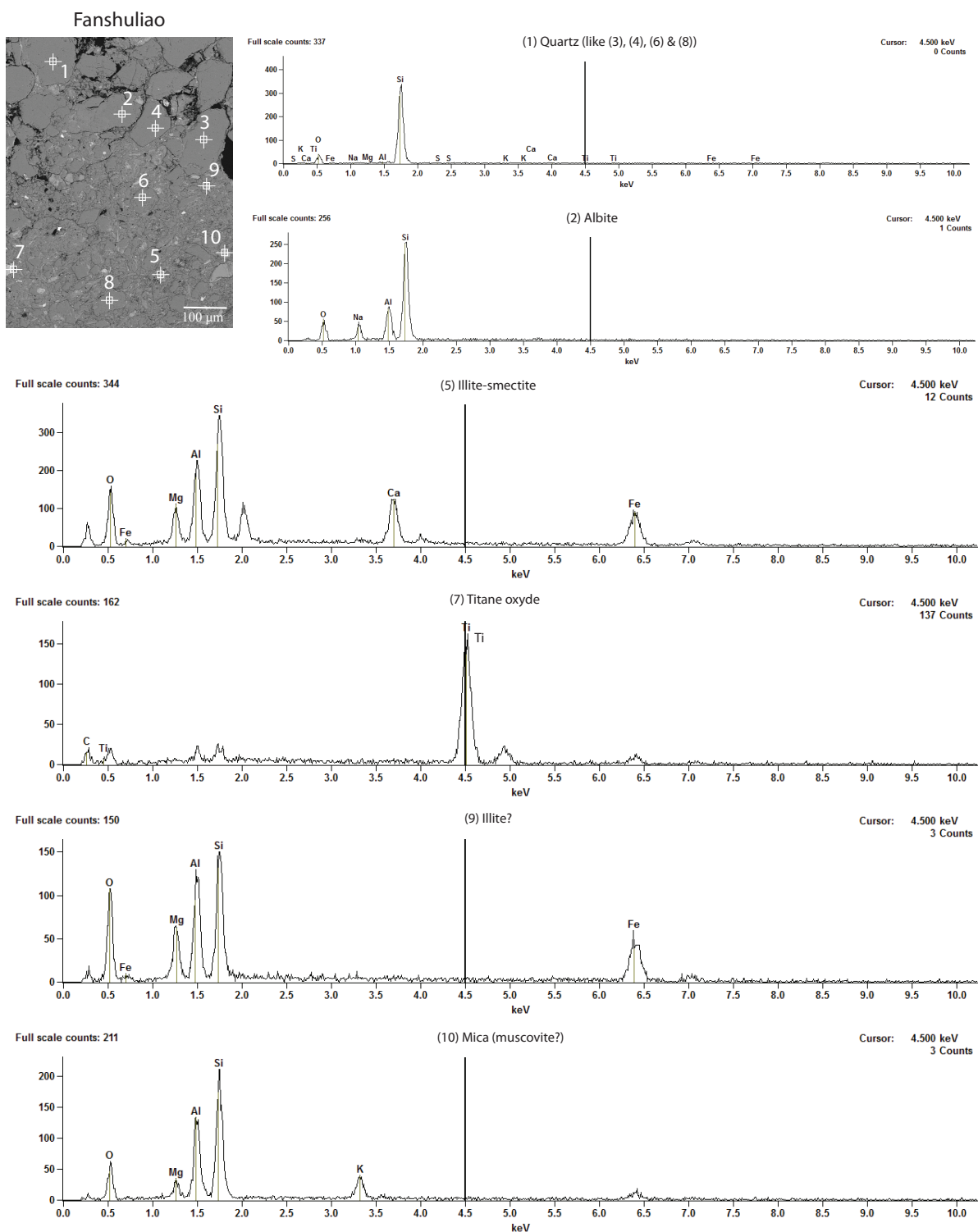


Figure S4: Representative EDS traces of grains inside the Fanshuliao formation, sample T12. For location of the analysis, see Figure 3.2d